

# 1 Theory

## 1.1 Three-band tight-binding model

In the model introduced by Liu *et al.*, only the orbitals of the M atom are included. We denote the wave functions of the three orbitals of the M atom as

$$|\phi_1\rangle = |d_{z^2}\rangle, \quad |\phi_2\rangle = |d_{xy}\rangle, \quad |\phi_3\rangle = |d_{x^2-y^2}\rangle. \quad (1)$$

The Bloch wavefunction in this model has the form

$$\psi_{\mathbf{k}}^\lambda(\mathbf{r}) = \sum_{j=1}^3 C_j^\lambda(\mathbf{k}) \sum_{\mathbf{R}} e^{i\mathbf{k}\cdot\mathbf{R}} \phi_j(\mathbf{r} - \mathbf{R}). \quad (2)$$

The coefficients  $C_j^\lambda(\mathbf{k})$  are the solutions of the eigenvalue equation

$$\sum_{jj'}^3 \left[ H_{jj'}^{\text{TB}}(\mathbf{k}) - \varepsilon_\lambda(\mathbf{k}) S_{jj'}(\mathbf{k}) \right] C_j^\lambda(\mathbf{k}) = 0, \quad (3)$$

where

$$H_{jj'}^{\text{TB}}(\mathbf{k}) = \sum_{\mathbf{R}} e^{i\mathbf{k}\cdot\mathbf{R}} \langle \phi_j(\mathbf{r}) | H_{1e} | \phi_{j'}(\mathbf{r} - \mathbf{R}) \rangle, \quad (4)$$

and

$$S_{jj'}(\mathbf{k}) = \sum_{\mathbf{R}} \langle \phi_j(\mathbf{r}) | \phi_{j'}(\mathbf{r} - \mathbf{R}) \rangle \approx \delta_{jj'}. \quad (5)$$

In the case  $B \neq 0$ , the new lattice vector now is  $\mathbf{R} = k\mathbf{a}_1 + l2q\mathbf{a}_2$ , where  $k, l \in \mathbb{Z}$ . The wavefunction has an additional phase factor

$$\psi_{\mathbf{k}}^\lambda(\mathbf{r}) = \sum_{j=1}^3 C_j^\lambda \sum_{\mathbf{R}} e^{i\mathbf{k}\cdot\mathbf{R}} e^{i\theta_{\mathbf{R}}(\mathbf{r})} \phi_j(\mathbf{r} - \mathbf{R}), \quad (6)$$

and choose  $\theta = -\frac{e}{\hbar} \int_{\mathbf{r}}^{\mathbf{R}} \mathbf{A}(\mathbf{r}') \cdot d\mathbf{r}'$  as Peierls phase factor, the Hamiltonian now is

$$H_{jj'} = \sum_{\mathbf{R}} e^{i\mathbf{k}\cdot\mathbf{R}} e^{\frac{ie}{\hbar} \int_0^{\mathbf{R}} \mathbf{A}(\mathbf{r}) \cdot d\mathbf{r}} E_{jj'}(\mathbf{R}), \quad (7)$$

where

$$E_{jj'} = \langle \phi_j(\mathbf{r}) | H_{1e} | \phi_{j'}(\mathbf{r} - \mathbf{R}) \rangle. \quad (8)$$

Using a uniform magnetic field  $\mathbf{B} = (0, 0, B)$  and Landau gauge  $\mathbf{A} = (By, 0, 0)$ . The

Peierls hopping phase is given

$$\begin{aligned} \frac{ie}{\hbar} \int_0^{\mathbf{R}} \mathbf{A}(\mathbf{r}) \cdot d\mathbf{r} &= \frac{ie}{\hbar} \int_0^{\mathbf{R}} B y dx \\ &= \frac{ieB}{\hbar} \int_0^1 y(\tau) x'(\tau) d\tau, \end{aligned} \quad (9)$$

suppose that the atom M is located at lattice vector  $\mathbf{R}_{m,n}$ , the Peierls phase can be written as

$$\theta_{m,n}^{m',n'} = \begin{cases} 0 & m' = m \pm 2, n' = n, \\ 0 & m' = m \pm 4, n' = n, \\ \pm \frac{e}{\hbar} \frac{Ba^2\sqrt{3}}{2} m & m' = m, n' = n \pm 2, \\ \pm \frac{e}{\hbar} \frac{Ba^2\sqrt{3}}{4} (m \mp \frac{1}{2}) & m' = m \mp 1, n' = n \pm 1, \\ \pm \frac{e}{\hbar} \frac{Ba^2\sqrt{3}}{2} (m \mp 1) & m' = m \mp 2, n' = n \pm 2, \\ \pm \frac{e}{\hbar} \frac{Ba^2\sqrt{3}}{4} (m \mp \frac{3}{2}) & m' = m \mp 3, n' = n \pm 1. \end{cases} \quad (10)$$

We obtain the Hamiltonian in magnetic field

$$\begin{aligned} H_{jj'}^{\text{TB}}(\mathbf{k}) &= E_{jj'}(\mathbf{0}) + e^{i\mathbf{k} \cdot \mathbf{R}_1} E_{jj'}(\mathbf{R}_1) + e^{-i\pi(m+1/2)\frac{\Phi}{\Phi_0}} e^{i\mathbf{k} \cdot \mathbf{R}_2} E_{jj'}(\mathbf{R}_2) \\ &+ e^{-i\pi(m-1/2)\frac{\Phi}{\Phi_0}} e^{i\mathbf{k} \cdot \mathbf{R}_3} E_{jj'}(\mathbf{R}_3) + e^{i\mathbf{k} \cdot \mathbf{R}_4} E_{jj'}(\mathbf{R}_4) \\ &+ e^{i\pi(m-1/2)\frac{\Phi}{\Phi_0}} e^{i\mathbf{k} \cdot \mathbf{R}_5} E_{jj'}(\mathbf{R}_5) + e^{i\pi(m+1/2)\frac{\Phi}{\Phi_0}} e^{i\mathbf{k} \cdot \mathbf{R}_6} E_{jj'}(\mathbf{R}_6) \\ &+ e^{-i\pi(m+3/2)\frac{\Phi}{\Phi_0}} e^{i\mathbf{k} \cdot \mathbf{R}_7} E_{jj'}(\mathbf{R}_7) + e^{-2i\pi m\frac{\Phi}{\Phi_0}} e^{i\mathbf{k} \cdot \mathbf{R}_8} E_{jj'}(\mathbf{R}_8) \\ &+ e^{-i\pi(m-3/2)\frac{\Phi}{\Phi_0}} e^{i\mathbf{k} \cdot \mathbf{R}_9} E_{jj'}(\mathbf{R}_9) + e^{i\pi(m-3/2)\frac{\Phi}{\Phi_0}} e^{i\mathbf{k} \cdot \mathbf{R}_{10}} E_{jj'}(\mathbf{R}_{10}) \\ &+ e^{2i\pi m\frac{\Phi}{\Phi_0}} e^{i\mathbf{k} \cdot \mathbf{R}_{11}} E_{jj'}(\mathbf{R}_{11}) + e^{i\pi(m+3/2)\frac{\Phi}{\Phi_0}} e^{i\mathbf{k} \cdot \mathbf{R}_{12}} E_{jj'}(\mathbf{R}_{12}) \\ &+ e^{i\mathbf{k} \cdot \mathbf{R}_{13}} E_{jj'}(\mathbf{R}_{13}) + e^{-2i\pi(m+1)\frac{\Phi}{\Phi_0}} e^{i\mathbf{k} \cdot \mathbf{R}_{14}} E_{jj'}(\mathbf{R}_{14}) \\ &+ e^{-2i\pi(m-1)\frac{\Phi}{\Phi_0}} e^{i\mathbf{k} \cdot \mathbf{R}_{15}} E_{jj'}(\mathbf{R}_{15}) + e^{i\mathbf{k} \cdot \mathbf{R}_{16}} E_{jj'}(\mathbf{R}_{16}) \\ &+ e^{2i\pi(m-1)\frac{\Phi}{\Phi_0}} e^{i\mathbf{k} \cdot \mathbf{R}_{17}} E_{jj'}(\mathbf{R}_{17}) + e^{2i\pi(m+1)\frac{\Phi}{\Phi_0}} e^{i\mathbf{k} \cdot \mathbf{R}_{18}} E_{jj'}(\mathbf{R}_{18}), \end{aligned} \quad (11)$$

where  $\Phi_0 = \frac{\hbar}{e}$  and  $\Phi = \frac{\sqrt{3}}{2} Ba^2$ . Since the Peierls phase depends on the the atomic position specified by the site indices  $m, n$ , the Hamiltonian is no longer invariant under translation of a primitive vector. For the case  $\frac{\Phi}{\Phi_0} = \frac{p}{q}$ , with  $p, q \in \mathbb{Z}$ , it is possible to restore the translational invariance if we expand the unit cell so that it includes  $2q$  M atoms. We, then, define a new basis set of  $6q$  atomic orbitals  $\{\phi_j(\mathbf{r} - \mathbf{R}_{m,n})\}$ . The wave

function can be expressed as the coefficients of  $C_{ji}^\lambda$  in the tight-binding wave function

$$\psi_{\mathbf{k}}^\lambda(\mathbf{r}) = \sum_j^3 \sum_i^{2q} C_{ji}^\lambda(\mathbf{k}) \sum_{\mathbf{R}} e^{\frac{ie}{\hbar} \int_0^{\mathbf{R}+\mathbf{R}_i} \mathbf{A}(\mathbf{r}) \cdot d\mathbf{r}} e^{i\mathbf{k} \cdot (\mathbf{R}+\mathbf{R}_i)} \phi_j(\mathbf{r} - \mathbf{R} - \mathbf{R}_i). \quad (12)$$

where  $j = 1, 2, 3$  and  $i$  labels the atom  $\mathbf{R}^{(i)}$  in the magnetic unit cell, with  $i = 1, \dots, 2q$ . In this basis, the TB Hamiltonian has an additional Peierls phase

$$H_{jij'i'} = \sum_{\mathbf{R}} e^{i\mathbf{k} \cdot (\mathbf{R}-\mathbf{R}_i+\mathbf{R}_{i'})} e^{\frac{ie}{\hbar} \int_{\mathbf{R}_i}^{\mathbf{R}+\mathbf{R}_{i'}} \mathbf{A}(\mathbf{r}) \cdot d\mathbf{r}} \langle \phi_j(\mathbf{r} - \mathbf{R}_i) | H_{1e} | \phi_{j'}(\mathbf{r} - \mathbf{R} - \mathbf{R}_{i'}) \rangle, \quad (13)$$

The sum over  $\mathbf{R}$  include up to third-nearest-neighbor hoppings. It is remarkable to note that the lattice vectors satisfying the condition  $|\mathbf{R}| \leq 2a$  are  $\mathbf{R} = \mathbf{0}, \pm\mathbf{a}_1, \pm 2\mathbf{a}_1$ , we obtain the Hamiltonian

$$\begin{aligned} H_{jnj'n'}^{\text{eff}}(\mathbf{k}) = & E_{jj'}(\mathbf{0})\delta_{n,n'} + e^{i\mathbf{k} \cdot \mathbf{R}_1} E_{jj'}(\mathbf{R}_1)\delta_{n,n'} + e^{i\mathbf{k} \cdot \mathbf{R}_4} E_{jj'}(\mathbf{R}_4)\delta_{n,n'} \\ & + e^{-i\pi(m+1/2)\frac{\Phi}{\Phi_0}} e^{i\mathbf{k} \cdot \mathbf{R}_2} E_{jj'}(\mathbf{R}_2)\delta_{n-1,n'} + e^{-i\pi(m-1/2)\frac{\Phi}{\Phi_0}} e^{i\mathbf{k} \cdot \mathbf{R}_3} E_{jj'}(\mathbf{R}_3)\delta_{n-1,n'} \\ & + e^{i\pi(m-1/2)\frac{\Phi}{\Phi_0}} e^{i\mathbf{k} \cdot \mathbf{R}_5} E_{jj'}(\mathbf{R}_5)\delta_{n+1,n'} + e^{i\pi(m+1/2)\frac{\Phi}{\Phi_0}} e^{i\mathbf{k} \cdot \mathbf{R}_6} E_{jj'}(\mathbf{R}_6)\delta_{n+1,n'} \\ & + e^{-i\pi(m+3/2)\frac{\Phi}{\Phi_0}} e^{i\mathbf{k} \cdot \mathbf{R}_7} E_{jj'}(\mathbf{R}_7)\delta_{n-1,n'} + e^{-2i\pi m\frac{\Phi}{\Phi_0}} e^{i\mathbf{k} \cdot \mathbf{R}_8} E_{jj'}(\mathbf{R}_8)\delta_{n-2,n'} \\ & + e^{-i\pi(m-3/2)\frac{\Phi}{\Phi_0}} e^{i\mathbf{k} \cdot \mathbf{R}_9} E_{jj'}(\mathbf{R}_9)\delta_{n-1,n'} + e^{i\pi(m-3/2)\frac{\Phi}{\Phi_0}} e^{i\mathbf{k} \cdot \mathbf{R}_{10}} E_{jj'}(\mathbf{R}_{10})\delta_{n+1,n'} \\ & + e^{2i\pi m\frac{\Phi}{\Phi_0}} e^{i\mathbf{k} \cdot \mathbf{R}_{11}} E_{jj'}(\mathbf{R}_{11})\delta_{n+2,n'} + e^{i\pi(m+3/2)\frac{\Phi}{\Phi_0}} e^{i\mathbf{k} \cdot \mathbf{R}_{12}} E_{jj'}(\mathbf{R}_{12})\delta_{n+1,n'} \\ & + e^{i\mathbf{k} \cdot \mathbf{R}_{13}} E_{jj'}(\mathbf{R}_{13})\delta_{n,n'} + e^{-2i\pi(m+1)\frac{\Phi}{\Phi_0}} e^{i\mathbf{k} \cdot \mathbf{R}_{14}} E_{jj'}(\mathbf{R}_{14})\delta_{n-2,n'} \\ & + e^{-2i\pi(m-1)\frac{\Phi}{\Phi_0}} e^{i\mathbf{k} \cdot \mathbf{R}_{15}} E_{jj'}(\mathbf{R}_{15})\delta_{n-2,n'} + e^{i\mathbf{k} \cdot \mathbf{R}_{16}} E_{jj'}(\mathbf{R}_{16})\delta_{n,n'} \\ & + e^{2i\pi(m-1)\frac{\Phi}{\Phi_0}} e^{i\mathbf{k} \cdot \mathbf{R}_{17}} E_{jj'}(\mathbf{R}_{17})\delta_{n+2,n'} + e^{2i\pi(m+1)\frac{\Phi}{\Phi_0}} e^{i\mathbf{k} \cdot \mathbf{R}_{18}} E_{jj'}(\mathbf{R}_{18})\delta_{n+2,n'}. \end{aligned} \quad (14)$$

where  $\Phi_0 = \frac{h}{e}$ ,  $\Phi = \frac{\sqrt{3}}{2}Ba^2$  and  $E(\mathbf{R})$  are obtained from Liu *et al.*

## 1.2 The cyclotron theory

The cyclotron frequency can be obtained from the energy difference between two Landau levels

$$\hbar\omega_c = E_{n+1} - E_n, \quad (15)$$

which gives

$$\omega_c = \frac{E_{n+1} - E_n}{\hbar}. \quad (16)$$

On the other hand, the cyclotron frequency is also defined as

$$\omega_c = \frac{eB}{m^*}. \quad (17)$$

Combining the two expressions, the effective mass can be written as

$$m^* = \frac{eB}{\omega_c} = \frac{eB}{\frac{E_{n+1}-E_n}{\hbar}} = \frac{eB\hbar}{E_{n+1} - E_n}. \quad (18)$$

## 2 Methods

When a magnetic field is applied to the crystal lattice, the magnetic unit cell is enlarged  $q$  times for square lattice ( $2q$  times for hexagonal lattice). As a consequence, the magnetic Brillouin zone is smaller  $2q$  times than the original Brillouin zone.

In addition, the three bases  $d_{z^2}, d_{xy}, d_{x^2-y^2}$ , which were introduced by Liu *et al.*, cannot clearly distinguish the  $K$  and  $K'$  points in the valence and conduction bands for two reasons. First, the squared amplitudes  $|\psi|^2$  are identical. Second, in the magnetic Brillouin zone, the  $K$  and  $K'$  valleys cannot be intuitively distinguished by the dispersion relation  $E(\mathbf{k})$ ; instead, one needs to examine the properties of the wave functions. Specifically, the electron wave function at the  $K$  valley is mainly contributed by  $d_{z^2}$ , while at the  $K'$  valley it is  $d_{xy} + d_{x^2-y^2}$ . Therefore, it is necessary to adopt another basis set. We now consider a new basis consisting of the three eigenfunctions of the angular momentum operators  $L^2$  and  $L_z$ , corresponding to  $l = 2$  and  $m = 0, \pm 2$ .

$$|\tilde{\phi}_1\rangle = |d_{m=0}\rangle, \quad |\tilde{\phi}_2\rangle = |d_{m=+2}\rangle, \quad |\tilde{\phi}_3\rangle = |d_{m=-2}\rangle. \quad (19)$$

The new basis can be obtained from the old one by the transformation

$$|\tilde{\phi}_j\rangle = \sum_{j'} W_{j'j} |\phi_{j'}\rangle, \quad (20)$$

where

$$W = \begin{pmatrix} 1 & 0 & 0 \\ 0 & \frac{i}{\sqrt{2}} & -\frac{i}{\sqrt{2}} \\ 0 & \frac{1}{\sqrt{2}} & \frac{1}{\sqrt{2}} \end{pmatrix}. \quad (21)$$

In particular,

$$|\tilde{\phi}_1\rangle = |\phi_1\rangle, \quad (22)$$

$$|\tilde{\phi}_2\rangle = \frac{i}{\sqrt{2}}|\phi_2\rangle + \frac{1}{\sqrt{2}}|\phi_3\rangle, \quad (23)$$

$$|\tilde{\phi}_3\rangle = -\frac{i}{\sqrt{2}}|\phi_2\rangle + \frac{1}{\sqrt{2}}|\phi_3\rangle. \quad (24)$$

The TB Hamiltonian in new basis reads

$$\tilde{H}^{\text{TB}}(\mathbf{k}) = W^\dagger H^{\text{TB}}(\mathbf{k}) W, \quad (25)$$

where  $H^{\text{TB}} = H^{\text{NN}}$  or  $H^{\text{TNN}}$ .

To distinguish the states that originate from the original Brillouin zone, we follow the convention of Ho *et al.* [1]. Each Landau level is then labeled as  $|j, n\rangle_\tau$ , where  $j$ ,  $n$ , and  $\tau$  denote the orbital, Landau, and valley indices, respectively.

When diagonalizing the Hamiltonian in Eq. (14), we obtain  $2q$  eigenvalues for each orbital  $\phi_j(\mathbf{r})$ , with  $j = 1, 2, 3$ . In total, this gives  $6q$  eigenvalues. The eigenvalues corresponding to the valence band range from 0 to  $2q$ , while those of the conduction band range from  $2q + 1$  to  $4q$ .

For instance, in Fig. 1(a), the first Landau level is labeled as  $|0, 0\rangle_{K'}$ . This level is degenerate, i.e.,  $E_{2q+1} = E_{2q+2}$ , corresponding to the same energy value. Similarly, the second Landau level is labeled as  $|0, 1\rangle_{K'}$ , which corresponds to the two degenerate eigenvalues  $E_{2q+3} = E_{2q+4}$ , and so on for the subsequent Landau levels. In Fig. 1(d), for the valence band, we clearly observe the evidence of the Brillouin zone shrinking. At a given value of  $B$ , the same energy value is obtained simultaneously at the  $K$ ,  $K'$ , and  $\Gamma$  points. The first Landau level in the valence band corresponds to the eigenvalue  $E_{2q}$  (labeled as  $|2, 0\rangle_{K'}$ ), which is degenerate with  $E_{2q-1}$ . The second Landau level then corresponds to  $E_{2q-2}$  and  $E_{2q-3}$ , and so on for the lower levels.

In terms of Eq. (22), we have

$$m_e^* = \frac{eB\hbar}{E_{2q+3} - E_{2q+1}}. \quad (26)$$

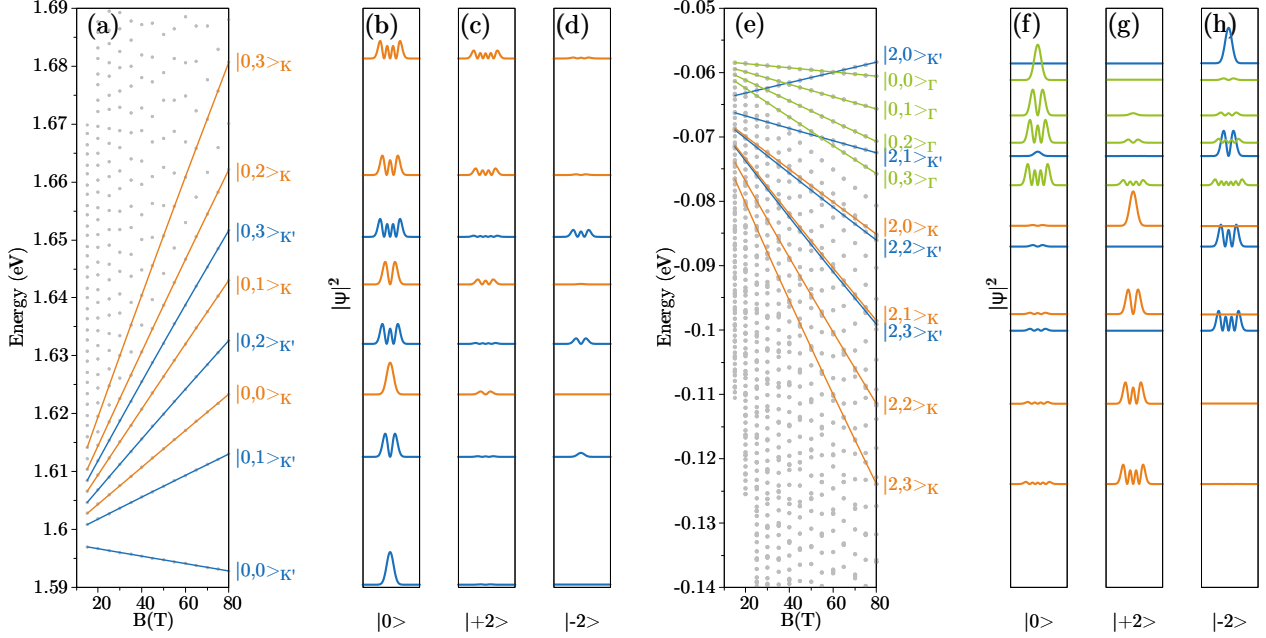
However, for  $m_h^*$ , the situation is quite different and more complicated than for  $m_e^*$ . This difficulty arises because the energy of the  $\Gamma$  point lies close to the  $K$  and  $K'$  valleys. As a consequence, in Fig. 1(d), the eigenvalues are no longer linear or follow the sequential index  $2q - n$  as in the case of  $m_e^*$ , but instead exhibit level crossings due to numerical

issues. To address this, first, we need to determine the energy value  $E_n$  at a given  $B$  that corresponds to the envelope function. This can be done by plotting all the wave functions from 0 to  $2q$ , since each wave function provides information about the Landau level labeling. From the wave functions, we can then identify which  $E_n$  corresponds to  $|j, n\rangle_\tau$ .

### 3 Numerical results

#### 3.1 Effective mass

##### Monolayer MoS<sub>2</sub>



Hình 1: Landau levels (a) and the corresponding envelope-function components (b),(c),(d) for conduction electrons at valleys  $K$  and  $K'$ . Figs (e)–(h) show the same as (a)–(d) but for valence electrons. (Recalculated from Ho *et al.* [1])

The band structure of MoS<sub>2</sub> without a magnetic field shows that, in the valence band, the  $\Gamma$  point has an energy level of  $E \approx -0.058$  eV. Therefore, when a magnetic field is applied, this  $\Gamma$ -point energy level still appears.

The effective masses of MoS<sub>2</sub> in the absence of a magnetic field, calculated from

$$\frac{1}{m_{ij}^*} = \frac{1}{\hbar^2} \frac{\partial^2 E(\mathbf{k})}{\partial k_i \partial k_j}, \quad (27)$$

are  $m_e \approx 0.4178m_0$ ,  $m_h \approx 0.5325m_0$ , and  $m_r \approx 0.2341$  for the TNN case, and  $m_e \approx 0.4508m_0$ ,  $m_h \approx 0.6487m_0$ , and  $m_r \approx 0.2659m_0$  for the NN case.

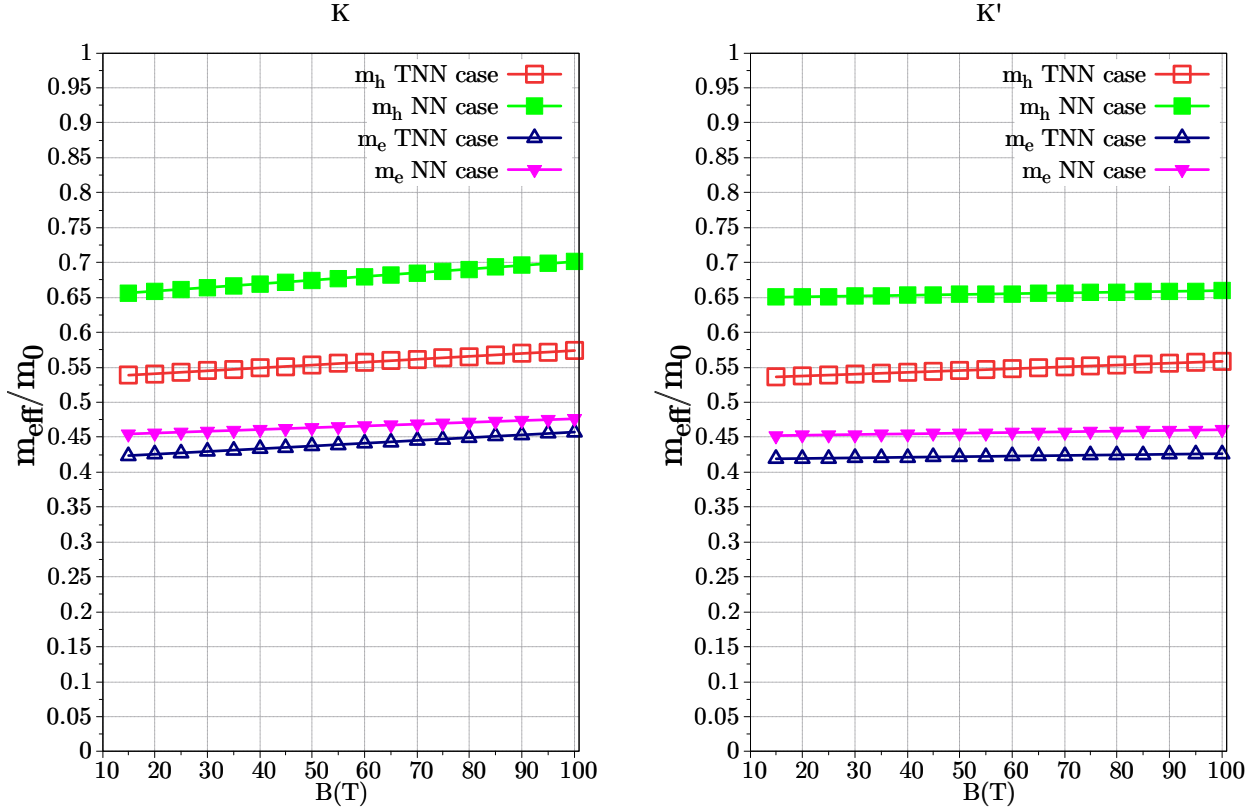
When a strong magnetic field is applied, for example  $B = 100$  T:

a) Nearest neighbor (NN)

- At valley  $K$ :  $m_h \approx 0.7011m_0$ ,  $m_e \approx 0.4763m_0$ . The reduced mass is  $m_r \approx 0.2836m_0$ , which increases by  $\approx 6.7\%$ .
- At valley  $K'$ :  $m_h \approx 0.6597m_0$ ,  $m_e \approx 0.4606m_0$ . The reduced mass is  $m_r \approx 0.2713m_0$ , which increases by  $\approx 2.0\%$ .

b) Third nearest neighbor (TNN)

- At valley  $K$ :  $m_h \approx 0.5739m_0$ ,  $m_e \approx 0.4573m_0$ . The reduced mass is  $m_r \approx 0.2545m_0$ , which increases by  $\approx 8.71\%$ .
- At valley  $K'$ :  $m_h \approx 0.5584m_0$ ,  $m_e \approx 0.4263m_0$ . The reduced mass is  $m_r \approx 0.2417m_0$ , which increases by  $\approx 3.25\%$ .

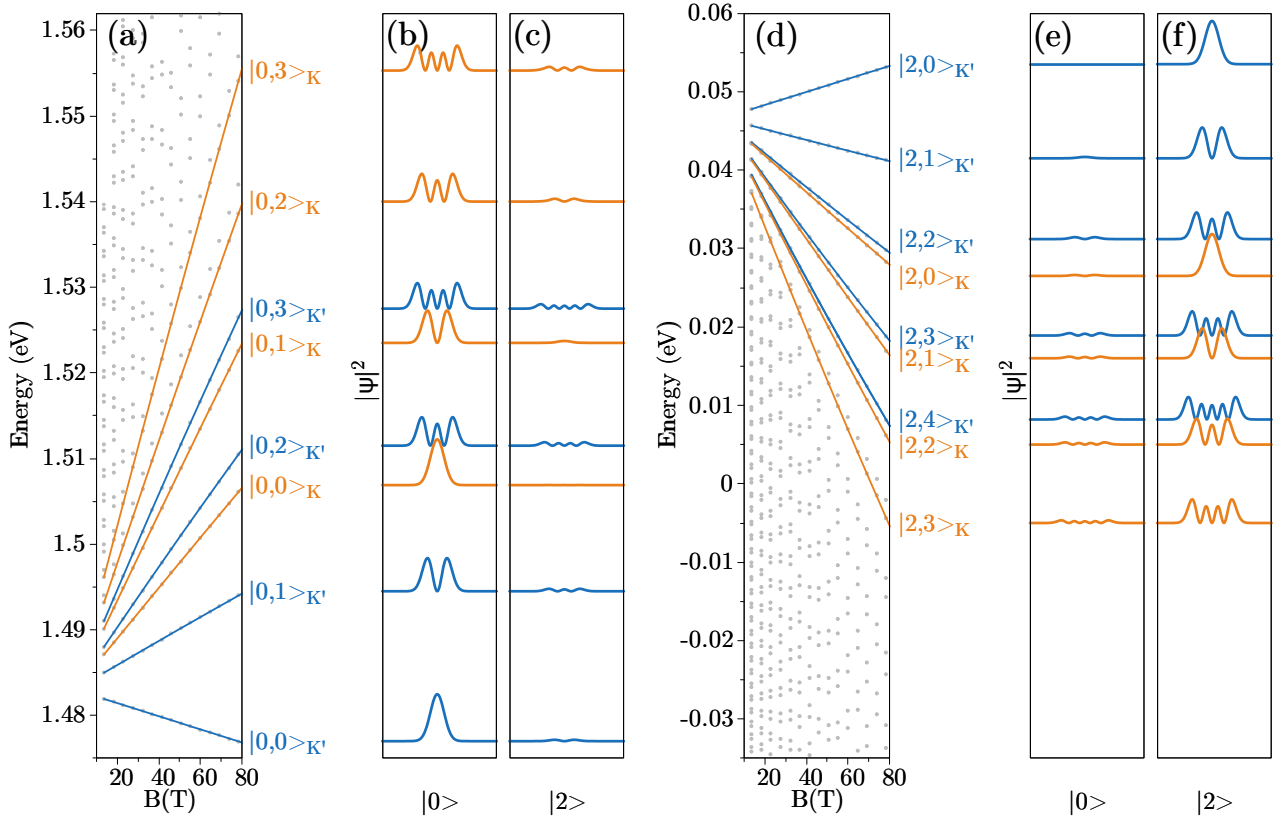


Hình 2: Effective masses.

Meanwhile, Goryca *et al.* [2] reported that  $m_r \approx 0.27 \pm 0.01m_0$ , which is 4% – 10.2% larger than the earlier result of Berkelbach *et al.* [3],  $m_r = 0.245 \pm 0.005m_0$ . Based on our calculations, we argue that the reduced mass at valley  $K$ ,  $m_r \approx 0.2545m_0$  with an increase of 8.71%, is consistent with the experimental findings of Goryca *et al.*.



## Monolayer MoSe<sub>2</sub>



Hình 3: Landau levels (a) and the corresponding envelope-function components (b),(c) for conduction electrons at valleys  $K$  and  $K'$ . Figs (d)–(f) show the same as (a)–(c) but for valence electrons.

The band structure of MoSe<sub>2</sub> without a magnetic field shows that the  $\Gamma$  point does not appear near the  $K$  point. Therefore, when a magnetic field is applied, the  $\Gamma$ -point energy level is absent in this region. In addition, the first three Landau levels originate from the  $K'$  valley, in contrast to WSe<sub>2</sub>, where the first two Landau levels originate from the  $K'$  valley.

The effective masses of MoSe<sub>2</sub> in the absence of a magnetic field, calculated from

$$\frac{1}{m_{ij}^*} = \frac{1}{\hbar^2} \frac{\partial^2 E(\mathbf{k})}{\partial k_i \partial k_j},$$

are  $m_e \approx 0.4770m_0$ ,  $m_h \approx 0.5887m_0$ , and  $m_r \approx 0.2634m_0$  for the TNN case, and  $m_e \approx 0.5226m_0$ ,  $m_h \approx 0.7512m_0$ , and  $m_r \approx 0.3082m_0$  for the NN case.

When a strong magnetic field is applied, for example  $B = 100$  T:

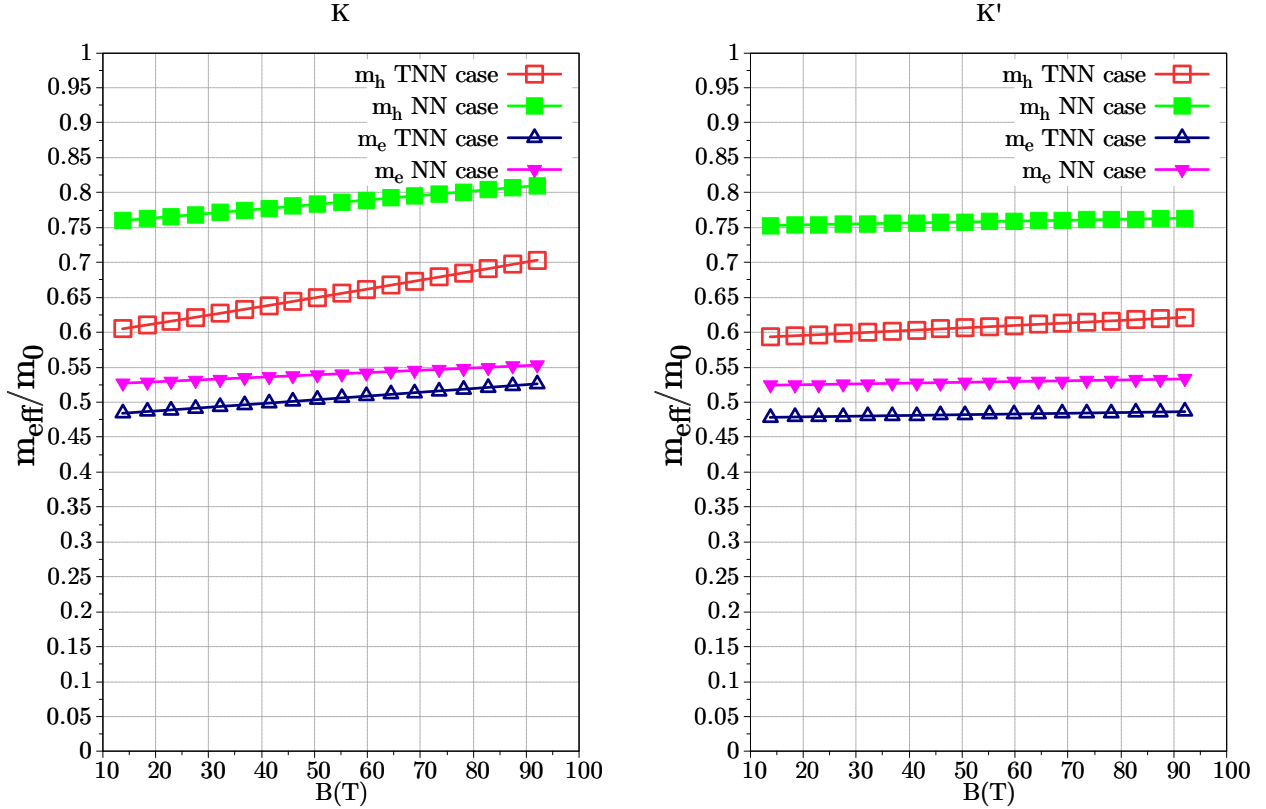
a) Nearest neighbor (NN)

- At valley  $K$ :  $m_h \approx 0.8100m_0$ ,  $m_e \approx 0.5529m_0$ . The reduced mass is  $m_r \approx 0.3286m_0$ , which increases by  $\approx 6.62\%$ .

- At valley  $K'$ :  $m_h \approx 0.7632m_0$ ,  $m_e \approx 0.5331m_0$ . The reduced mass is  $m_r \approx 0.3138m_0$ , which increases by  $\approx 1.82\%$ .

b) Third nearest neighbor (TNN)

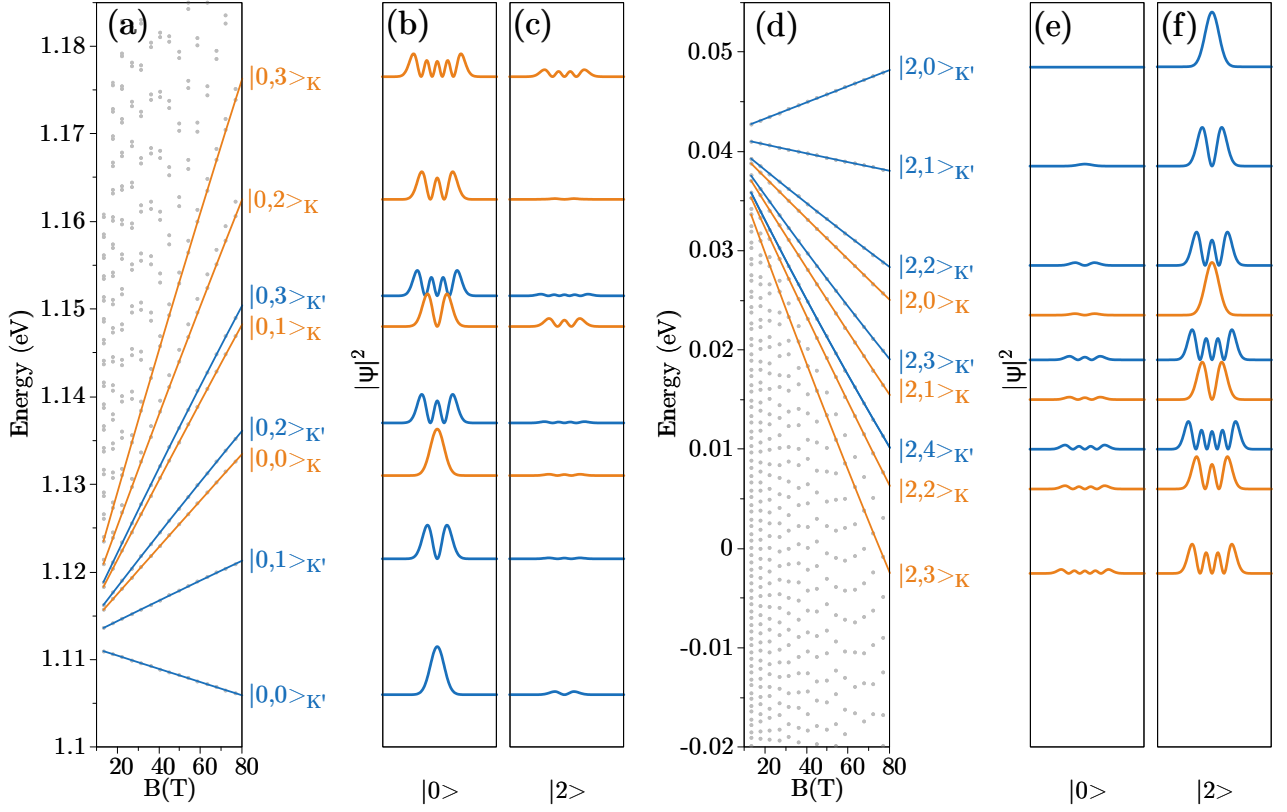
- At valley  $K$ :  $m_h \approx 0.7168m_0$ ,  $m_e \approx 0.5320m_0$ . The reduced mass is  $m_r \approx 0.3052m_0$ , which increases by  $\approx 15.87\%$ .
- At valley  $K'$ :  $m_h \approx 0.6251m_0$ ,  $m_e \approx 0.4874m_0$ . The reduced mass is  $m_r \approx 0.2738m_0$ , which increases by  $\approx 3.95\%$ .



Hình 4: Effective masses.

Meanwhile, Goryca *et al.* [2] reported that  $m_r \approx 0.350 \pm 0.015m_0$ , which is 24.1% – 35.2% larger than the earlier result of Berkelbach *et al.* [3],  $m_r = 0.27m_0$ . Based on our calculations, we argue that at valley  $K$ , the reduced mass  $m_r \approx 0.3052m_0$ , with an increase of 15.87%, does not fully agree with the experimental findings of Goryca *et al.*.

## Monolayer MoTe<sub>2</sub>



Hình 5: Landau levels (a) and the corresponding envelope-function components (b),(c) for conduction electrons at valleys  $K$  and  $K'$ . Panels (d)–(f) show the same as (a)–(c) but for valence electrons..

The band structure of MoTe<sub>2</sub> without a magnetic field shows that the  $\Gamma$  point has an energy level of  $E \approx -0.1075$  eV. Therefore, when a magnetic field is applied, this  $\Gamma$ -point energy level still appears.

The effective masses of MoTe<sub>2</sub> in the absence of a magnetic field, calculated from

$$\frac{1}{m_{ij}^*} = \frac{1}{\hbar^2} \frac{\partial^2 E(\mathbf{k})}{\partial k_i \partial k_j},$$

are  $m_e \approx 0.4318m_0$ ,  $m_h \approx 0.6044m_0$ , and  $m_r \approx 0.2519m_0$  for the TNN case, and  $m_e \approx 0.5913m_0$ ,  $m_h \approx 0.8975m_0$ , and  $m_r \approx 0.3565m_0$  for the NN case, as also reported by Goryca *et al.* [2]. Among the six materials considered, MoTe<sub>2</sub> has the largest effective masses  $m_e$  and  $m_h$  in the absence of a magnetic field.

When a strong magnetic field is applied, for example  $B = 90$  T:

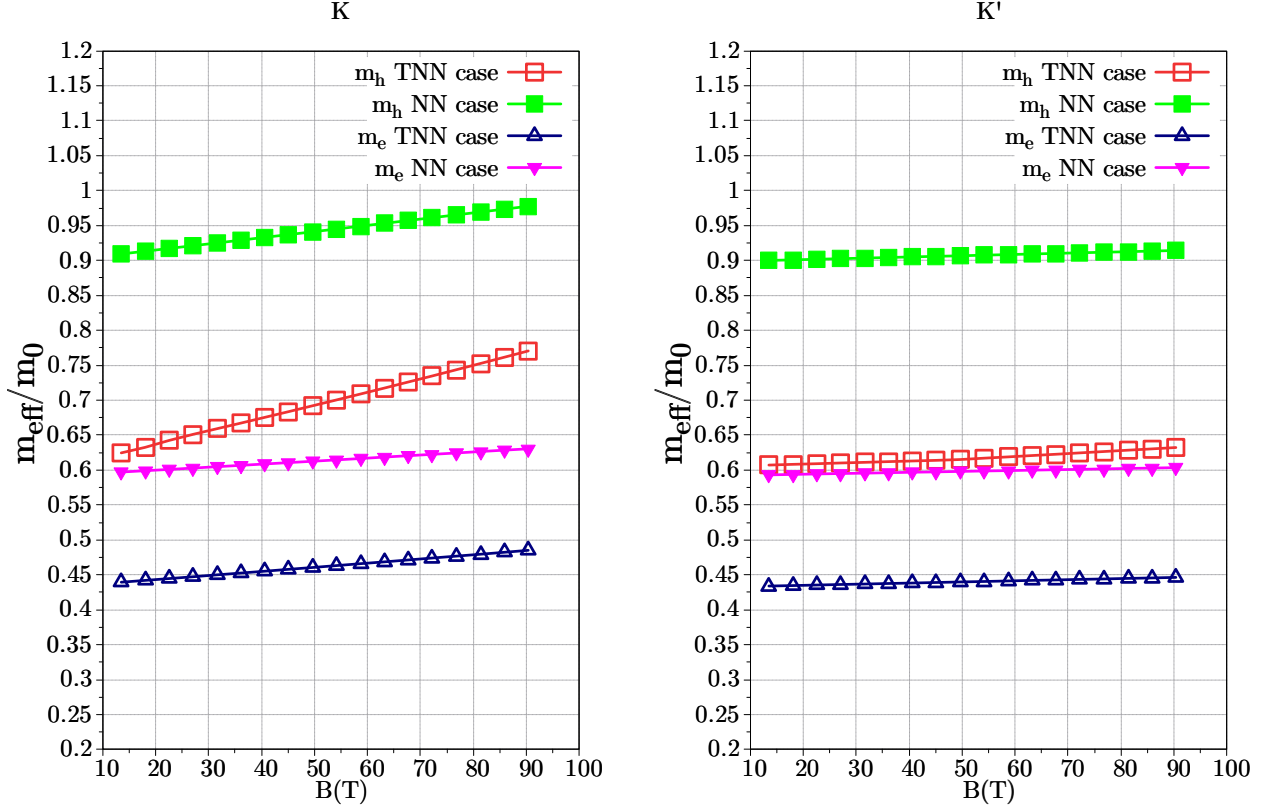
a) Nearest neighbor (NN)

- At valley  $K$ :  $m_h \approx 0.9774m_0$ ,  $m_e \approx 0.6304m_0$ . The reduced mass is  $m_r \approx 0.3832m_0$ , which increases by  $\approx 7.49\%$ .

- At valley  $K'$ :  $m_h \approx 0.9142m_0$ ,  $m_e \approx 0.6034m_0$ . The reduced mass is  $m_r \approx 0.3635m_0$ , which increases by  $\approx 1.96\%$ .

b) Third nearest neighbor (TNN)

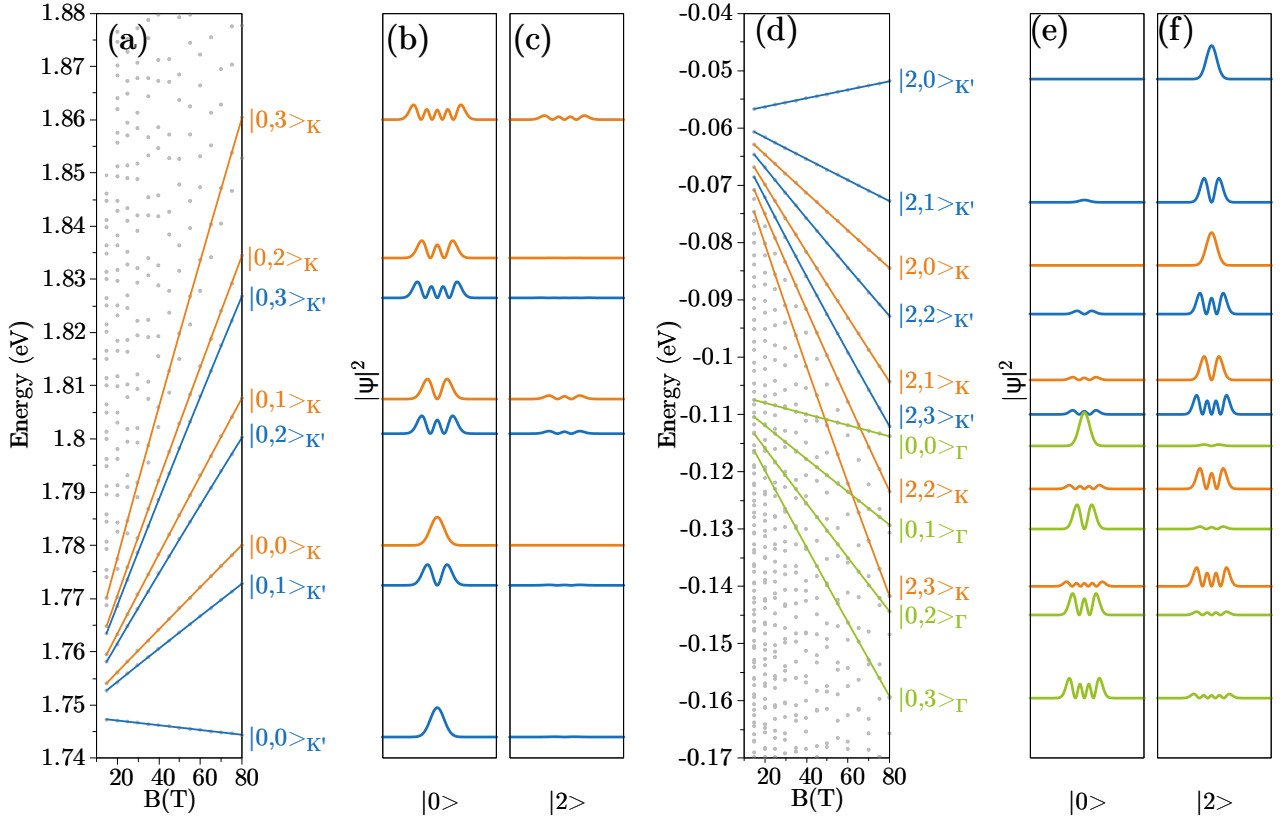
- At valley  $K$ :  $m_h \approx 0.7704m_0$ ,  $m_e \approx 0.4850m_0$ . The reduced mass is  $m_r \approx 0.2976m_0$ , which increases by  $\approx 18.14\%$ .
- At valley  $K'$ :  $m_h \approx 0.6322m_0$ ,  $m_e \approx 0.4463m_0$ . The reduced mass is  $m_r \approx 0.2616m_0$ , which increases by  $\approx 3.85\%$ .



Hình 6: Effective masses.

In the study of Goryca *et al.* [2], the reduced mass was reported as  $m_r = 0.36 \pm 0.04m_0$ , which is about 25% larger than the value obtained in the work of Kormányos *et al.* [4]. In our case, for the TNN model, the reduced mass is  $m_r = 0.2976m_0$ , which increases by  $\approx 18\%$  compared to the zero-field value  $m_r = 0.2519m_0$ .

## Monolayer WS<sub>2</sub>



Hình 7: Landau levels (a) and the corresponding envelope-function components (b),(c) for conduction electrons at valleys  $K$  and  $K'$ . Panels (d)–(f) show the same as (a)–(c) but for valence electrons.

The band structure of WS<sub>2</sub> without a magnetic field shows that the  $\Gamma$  point has an energy level of  $E \approx -0.1075$  (eV). Therefore, when a magnetic field is applied, the energy level at the  $\Gamma$  point still appears.

The effective mass of WS<sub>2</sub> without a magnetic field, calculated using

$$\frac{1}{m_{ij}^*} = \frac{1}{\hbar^2} \frac{\partial^2 E(\mathbf{k})}{\partial k_i \partial k_j},$$

yields  $m_e \approx 0.2956m_0$ ,  $m_h \approx 0.3845m_0$ ,  $m_r \approx 0.1671m_0$  in the TNN case, and  $m_e \approx 0.3195m_0$ ,  $m_h \approx 0.4348m_0$ ,  $m_r \approx 0.1841m_0$  in the NN case.

For a strong magnetic field, e.g.,  $B = 100$  T:

a) Nearest neighbor

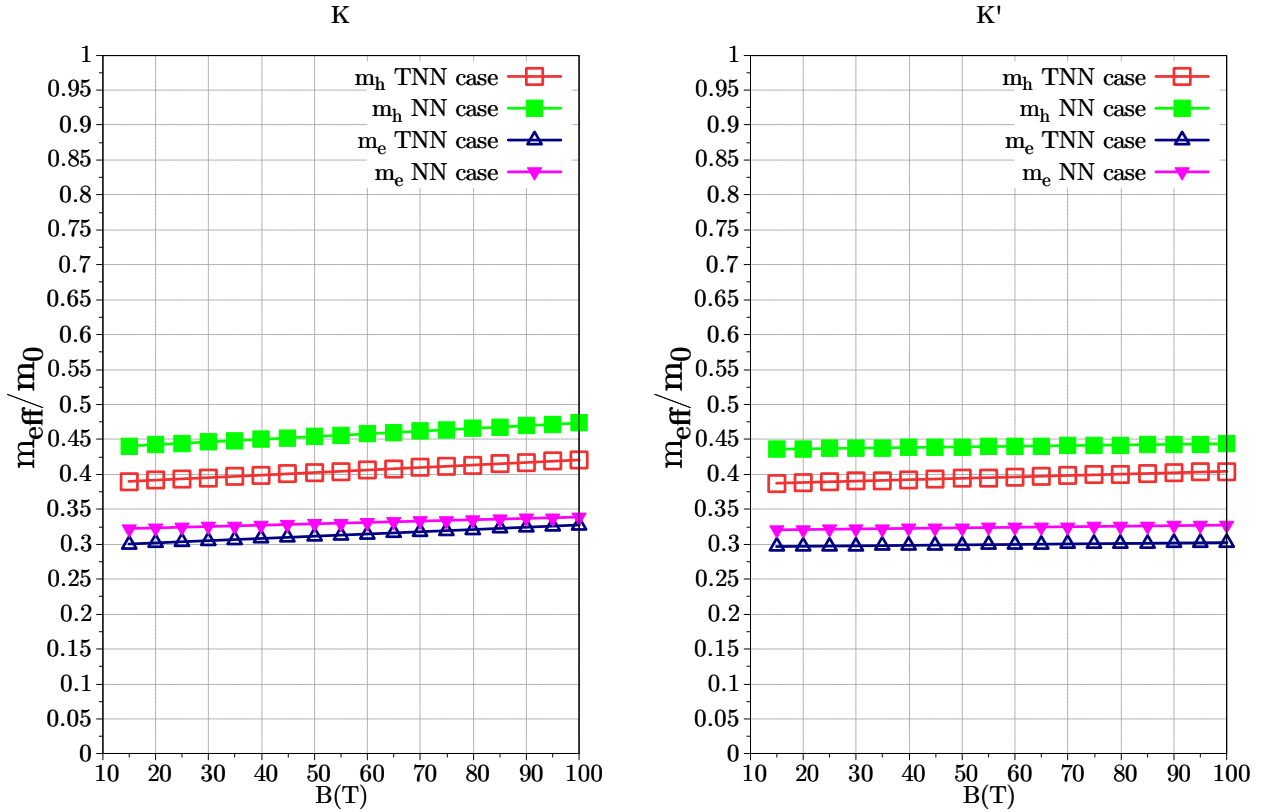
- At the  $K$  valley:  $m_h \approx 0.4735m_0$ ,  $m_e \approx 0.3389m_0$ . Thus,  $m_r \approx 0.1974m_0$ , which increases by  $\approx 7.2\%$ .
- At the  $K'$  valley:  $m_h \approx 0.4438m_0$ ,  $m_e \approx 0.3273m_0$ . Thus,  $m_r \approx 0.1885m_0$ , which increases by  $\approx 2.3\%$ .

b) Third nearest neighbor

- At the K valley:  $m_h \approx 0.4205m_0$ ,  $m_e \approx 0.3275m_0$ . Thus,  $m_r \approx 0.1841m_0$ , which increases by  $\approx 10.17\%$ .
- At the K' valley:  $m_h \approx 0.4043m_0$ ,  $m_e \approx 0.3023m_0$ . Thus,  $m_r \approx 0.1730m_0$ , which increases by  $\approx 3.53\%$ .

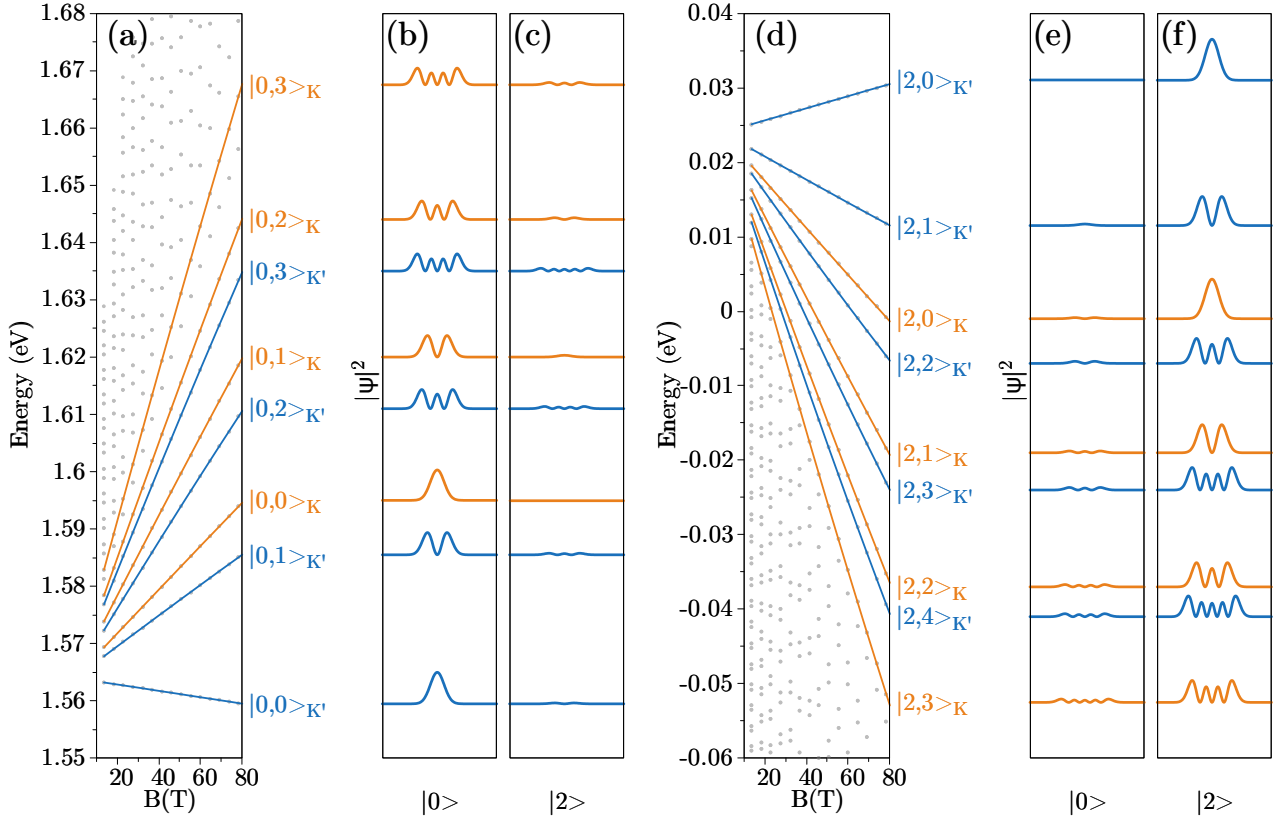
In the study of Goryca *et al.* [2], they reported  $m_r = 0.175 \pm 0.007m_0$ , which is about 10% larger than the value  $m_r = 0.15 - 0.16m_0$  obtained in the work of Berkelbach *et al.* [3].

In our case, for the K valley under the TNN approximation, we obtain  $m_r \approx 0.1841m_0$  in the presence of a magnetic field, which corresponds to an increase of  $\approx 10\%$  compared to  $m_r \approx 0.1671m_0$  without a magnetic field. This result is consistent with and reasonable compared to the experimental findings of Goryca *et al.* [2].



Hình 8: Khối lượng hiệu dụng.

## Monolayer WSe<sub>2</sub>



Hình 9: Landau levels (a) and the corresponding envelope-function components (b),(c) for conduction electrons at valleys  $K$  and  $K'$ . Panels (d)–(f) show the same as (a)–(c) but for valence electrons.

The band structure of WSe<sub>2</sub> without a magnetic field shows that the  $\Gamma$  point lies much lower in energy than the  $K$  point. Therefore, when a magnetic field is applied, the energy level at the  $\Gamma$  point does not appear here.

The effective mass of WSe<sub>2</sub> without a magnetic field, calculated using

$$\frac{1}{m_{ij}^*} = \frac{1}{\hbar^2} \frac{\partial^2 E(\mathbf{k})}{\partial k_i \partial k_j},$$

yields  $m_e \approx 0.3124m_0$ ,  $m_h \approx 0.4022m_0$ ,  $m_r \approx 0.1758m_0$  in the TNN case, and  $m_e \approx 0.3487m_0$ ,  $m_h \approx 0.4792m_0$ ,  $m_r \approx 0.2018m_0$  in the NN case, as reported in the works of Kylänpää *et al.* and Berkelbach *et al.* [5, 3].

For a strong magnetic field, e.g.,  $B = 100$  T:

a) Nearest neighbor

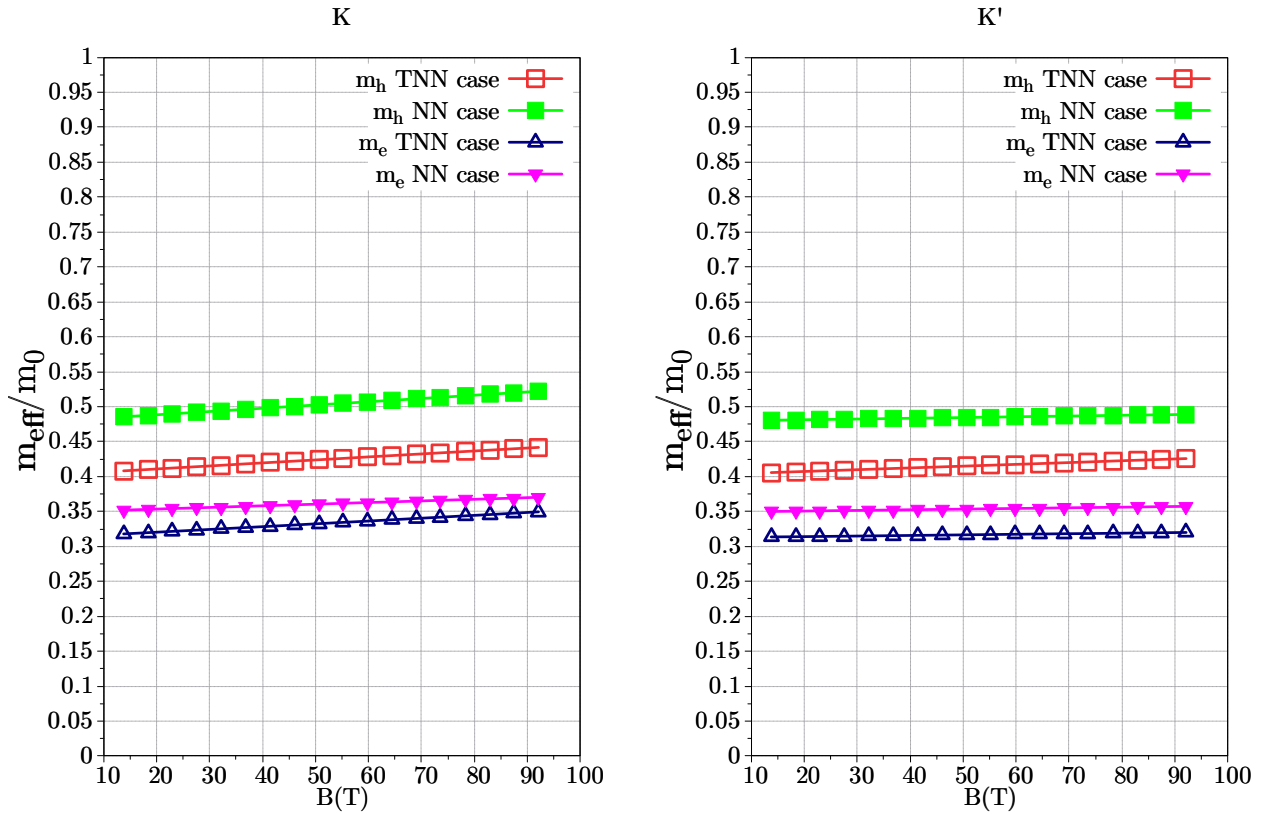
- At the  $K$  valley:  $m_h \approx 0.5220m_0$ ,  $m_e \approx 0.3702m_0$ . Thus,  $m_r \approx 0.2166m_0$ , which increases by  $\approx 7.34\%$ .
- At the  $K'$  valley:  $m_h \approx 0.4888m_0$ ,  $m_e \approx 0.3573m_0$ . Thus,  $m_r \approx 0.2064m_0$ ,

which increases by  $\approx 2.28\%$ .

b) Third nearest neighbor

- At the K valley:  $m_h \approx 0.4417m_0$ ,  $m_e \approx 0.3494m_0$ . Thus,  $m_r \approx 0.1951m_0$ , which increases by  $\approx 10.98\%$ .
- At the K' valley:  $m_h \approx 0.4257m_0$ ,  $m_e \approx 0.3199m_0$ . Thus,  $m_r \approx 0.1826m_0$ , which increases by  $\approx 3.87\%$ .

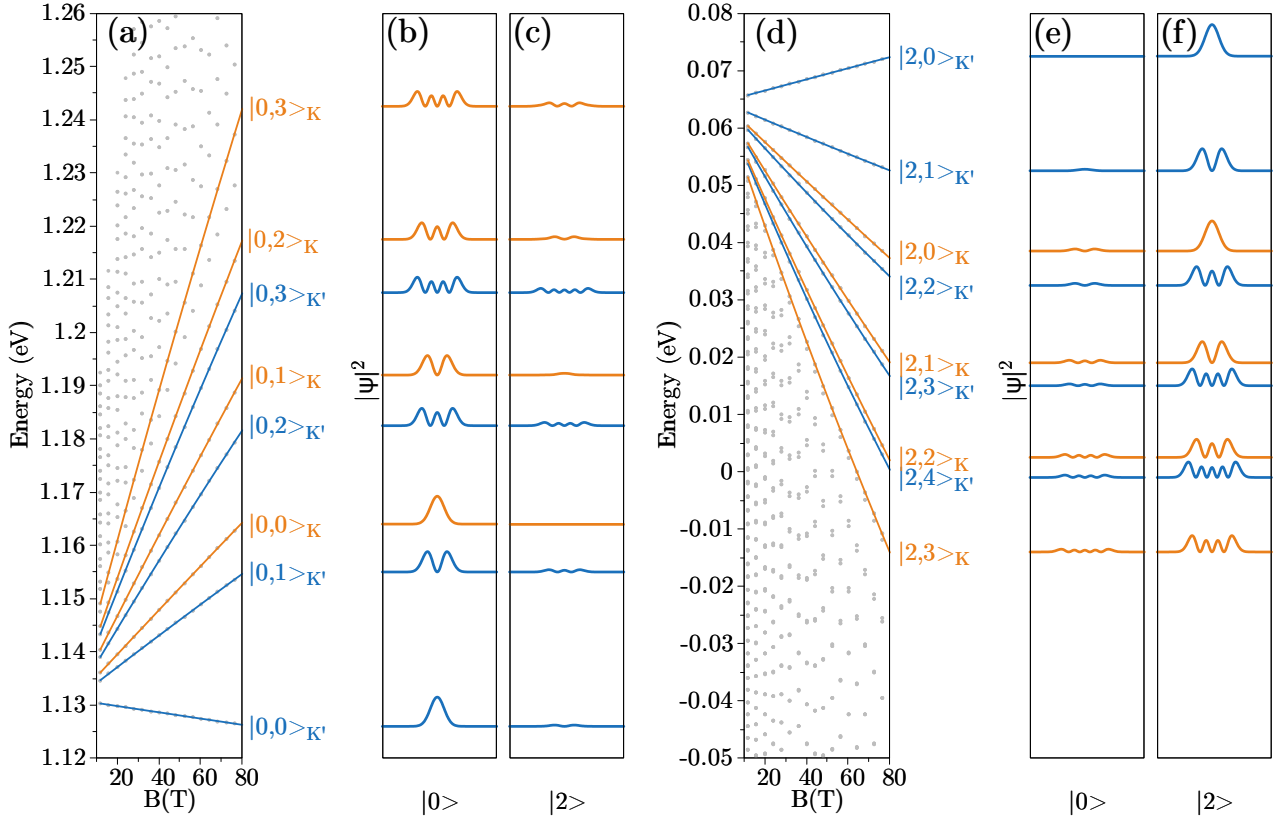
In the study of Stier *et al.* [6], they reported  $m_r \approx 0.20 \pm 0.01m_0$ , which is about 15% larger than the predictions of recent theoretical works [3, 5]. In our case, for the K valley under the TNN approximation, we obtain  $m_r \approx 0.1951m_0$  in the presence of a magnetic field, corresponding to an increase of  $\approx 11\%$  compared to the value without a magnetic field. This result is consistent with the findings reported by Stier *et al.* [6].



Hình 10: Khối lượng hiệu dụng.



## Monolayer WTe<sub>2</sub>



Hình 11: Landau levels (a) and the corresponding envelope-function components (b),(c) for conduction electrons at valleys  $K$  and  $K'$ . Panels (d)–(f) show the same as (a)–(c) but for valence electrons.

The band structure of WTe<sub>2</sub> in the absence of a magnetic field shows that the  $\Gamma$  point lies significantly lower in energy than the  $K$  point. Therefore, under an applied magnetic field, the Landau levels associated with the  $\Gamma$  point do not appear in this regime.

The effective masses of WTe<sub>2</sub> without a magnetic field, calculated using the formula  $\frac{1}{m_{ij}^*} = \frac{1}{\hbar^2} \frac{\partial^2 E(\mathbf{k})}{\partial k_i \partial k_j}$ , are found to be  $m_e \approx 0.2478m_0$ ,  $m_h \approx 0.3332m_0$ , and  $m_r \approx 0.1421m_0$  for the TNN case, and  $m_e \approx 0.3169m_0$ ,  $m_h \approx 0.4559m_0$ , and  $m_r \approx 0.187m_0$  for the NN case. To the best of our knowledge, no previous studies have reported the effective masses of WTe<sub>2</sub>.

At a high magnetic field, for example  $B = 80$  T, the effective masses are obtained as follows:

a) Nearest neighbor

– At the  $K$  valley:  $m_h \approx 0.5093m_0$ ,  $m_e \approx 0.3413m_0$ .

This yields  $m_r \approx 0.2044m_0$ , corresponding to an increase of  $\approx 9.3\%$ .

– At the  $K'$  valley:  $m_h \approx 0.4681m_0$ ,  $m_e \approx 0.3264m_0$ .

This gives  $m_r \approx 0.1923m_0$ , corresponding to an increase of  $\approx 2.83\%$ .

b) Third nearest neighbor

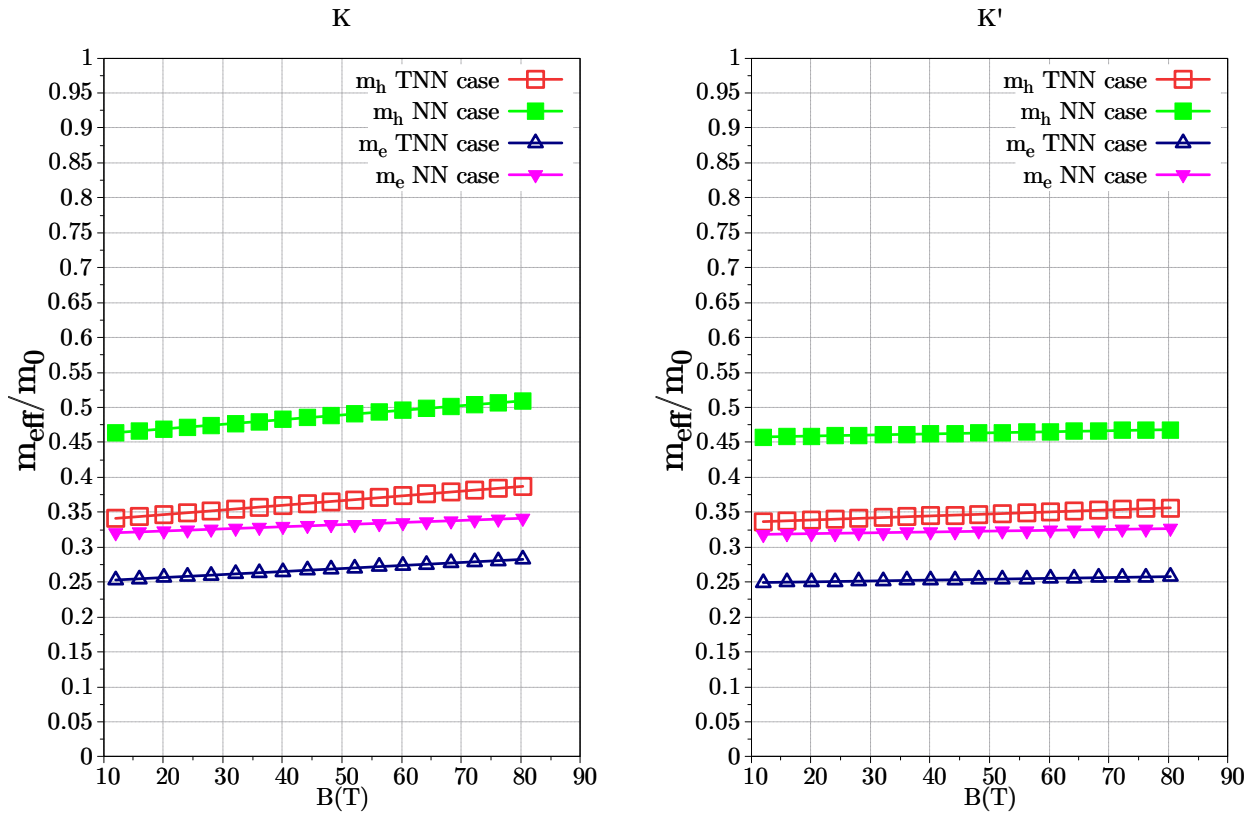
– At the K valley:  $m_h \approx 0.387m_0$ ,  $m_e \approx 0.2824m_0$ .

This yields  $m_r \approx 0.1633m_0$ , corresponding to an increase of  $\approx 14.92\%$ .

– At the K' valley:  $m_h \approx 0.3562m_0$ ,  $m_e \approx 0.2577m_0$ .

This gives  $m_r \approx 0.1495m_0$ , corresponding to an increase of  $\approx 5.21\%$ .

Thus, at the K valley in the TNN case, the reduced mass  $m_r$  of WTe<sub>2</sub> exhibits an increasing of nearly 15% under a strong magnetic field, which is consistent with the trend observed for other materials discussed above.



Hình 12: Khối lượng hiệu dụng.

# Tài liệu

- [1] Yen-Hung Ho, Yi-Hua Wang, and Hong-Yi Chen. Magneto-electronic and optical properties of a mos 2 monolayer. *Physical Review B*, 89(15):155316, 2014.
- [2] Mateusz Goryca, Jing Li, Andreas V Stier, Takashi Taniguchi, Kenji Watanabe, Emmanuel Courtade, Shivangi Shree, Cedric Robert, Bernhard Urbaszek, Xavier Marie, et al. Revealing exciton masses and dielectric properties of monolayer semiconductors with high magnetic fields. *Nature communications*, 10(1):4172, 2019.
- [3] Timothy C Berkelbach, Mark S Hybertsen, and David R Reichman. Theory of neutral and charged excitons in monolayer transition metal dichalcogenides. *Physical Review B—Condensed Matter and Materials Physics*, 88(4):045318, 2013.
- [4] Andor Kormányos, Guido Burkard, Martin Gmitra, Jaroslav Fabian, Viktor Zólyomi, Neil D Drummond, and Vladimir Fal’ko.  $k \cdot p$  theory for two-dimensional transition metal dichalcogenide semiconductors. *2D Materials*, 2(2):022001, 2015.
- [5] Ilkka Kylänpää and Hannu-Pekka Komsa. Binding energies of exciton complexes in transition metal dichalcogenide monolayers and effect of dielectric environment. *Physical Review B*, 92(20):205418, 2015.
- [6] Andreas V Stier, Nathan P Wilson, Kirill A Velizhanin, Junichiro Kono, Xiaodong Xu, and Scott A Crooker. Magneto-optics of exciton rydberg states in a monolayer semiconductor. *Physical review letters*, 120(5):057405, 2018.